CHAPTER 4
MECHANISM OF FAILURE SURFACE GROWTH IN SLOPE AFTER MINING

4.1 SUMMARY

This chapter deals with possible mechanisms of fracture extension and coalescence that must take place along the shale-middle coal seam contact to result in the observed mine slope collapses. Fracture extension is encouraged by stress relaxation normal to sedimentation due to open pit mining, discussed in the previous chapter. Many authors state that fracture initiation and possible extension are related to the pore size of the rock. The shales, which represent the weak layers in the slope profile, have very low porosity, ranging between 3% and 6%. Microscope study of thin sections together with X-ray analysis agree that the shales in the succession are polymineralic, laminated rocks, which include minerals both stronger and weaker than the surrounding muddy matrix. The most important of these minerals appear to be quartz and carbon, which appear as fragments and flakes usually larger than the grain size of the matrix in which they are set.

The significance of these minerals and their distribution is studied using of the Dugdale-Barenblatt analysis model (Dugdale, 1960; Barenblatt, 1962), in which collinear flaws represented by the carbon flakes coalesce to form a failure surface favourable to eventual slope collapse. Instead of a completely damaged zone with finite size, the model assumes that a

fracture process zone of macroscopically negligible width forms ahead of the tip of a Mode-I flaw, represented by the carbon flakes. Under the assumption of plane stress, a periodic array of collinear flaws (carbon flakes) with equal length is taken as an example of analysis. The critical length of the fracture process zone is assumed to be a rock constant, as is verified by the analysis of the increased distance between the flakes. The flaw coalescence is attributable to two causes: flaw propagation due to the mining-induced stress changes; and the linking of fracture process zones due to the small distance between neighbouring flakes, which promotes the development of the failure surfaces seen in the slope collapses.

4.2 INTRODUCTION

When rock is loaded to failure, cracks nucleate and propagate from pre-existing inhomogeneities, which can be in the form of pores, fractures, inclusions or other defects. The first plausible theoretical description of crack initiation and propagation in solids appeared in the early 1920s (Griffith 1921, 1924). Systematic theoretical and experimental investigations of crack initiation, propagation, and interaction in rock began in about the middle of the twentieth century and have continued since (Hoek and Bieniawski, 1965; Peng and Johnson, 1972; Hallbauer et al, 1973; Tapponnier and Brace, 1976; Olsson and Peng, 1976; Kranz, 1979; Batzle et al., 1980; Dey and Wang, 1981; Wong, 1982; Nemat-Nasser and Horii, 1982; Steif, 1984; Horii and Nemat-Nasser, 1985 and 1986; Ashby and Hallam, 1986; Sammis

and Ashby, 1986; Kemeny and Cook, 1987). It is recognised that under the combined action of tension and shear loading, both tensile and shear stress concentrations can develop at pre-existing inhomogeneities in rock. As the tension applied to the rock further increases, tensile cracks will be initiated. In the shear sliding crack model, this tensile crack is known as a "wing crack", which initiates from the tip of a pre-existing fracture and grows progressively in the direction normal to maximum tension. In the early stages, when the wing crack is short, the stress field around the pre-existing fracture from which it grows dominates the growth. As the crack extends, it starts to interact with neighbouring microcracks, and this interaction ultimately leads to crack coalescence and final failure of the sample (Ashby and Hallam, 1986).

Owing to the importance of the near crack-tip field in fracture behaviour, crack-inclusion interaction studies have received a great deal of attention in fracture mechanics (Lipetzky and Schmauder, 1994; Lipetzky and Knesl, 1995; Papaioannou and Hilton, 1974; Wang et al., 1998; Tamate, 1968; Helsing, 1999; Muller and Schmauder, 1993; Sih et al., 1970). Most of the studies use numerical approaches, such as the finite element method (Lipetzky and Schmauder, 1994; Lipetzky and Knesl, 1995; Papaioannou and Hilton, 1974), the boundary element method (Lipetzky and Knesl, 1995; Wang et al., 1998), and the singular integral equation method (Tamate, 1968; Helsing, 1999; Muller and Schmauder, 1993). A wide range of crack and inclusion geometries have been investigated by these numerical

analyses to show the effects of inclusion shape, size, location and stiffness in the near crack-tip field.
Some important work has been carried out using the numerical simulations of crack propagation and coalescence between multiple crack-like flaws. Using the Displacement Discontinuity Method (DDM), Scavia and Castelli (1996) and Scavia (1999) conducted some preliminary work, using a numerical technique to investigate the mechanical behaviour of rock bridges in material containing two and three crack-like flaws. In these studies, a series of numerical analyses was carried out to evaluate the influence of overlapping so as to identify a critical value for the resistance of the rock bridge between two cracks. The results show that direct and induced tensile crack propagation can occur in both stable and unstable conditions depending on flaw spacing and applied confining stresses. Vasarhelyi and Bobet (2000) have used the displacement discontinuity model, FROCK, to model crack initiation, propagation, and coalescence between two bridged flaws in gypsum under uniaxial compression. Their simulations reproduced the types of coalescence observed in the experiments, and they predicted an increase in coalescence stresses with increases in the bridged length. These inclusions have different shapes and stiffnesses, which affect the crack-tip field. The extent to which the near-tip field will be reduced or increased by the loading is dependent both on the stiffness difference between the inclusion and matrix and the inclusion geometry.

In most brittle and quasi-brittle materials such as concrete and rocks, damage evolution is typically attributable to nucleation, propagation, and

coalescence of microcracks. This process is very often anisotropic depending upon, for example, the loading history of external stresses. Several phenomenological and micromechanical damage models have been established for microcrack-weakened materials, for example Nemat-Nasser and Horii (1993), and Krajcinovic (1997).

To analyse and describe the fracture of various materials subjected to mechanical loads, various different methods have been developed. Among others, the Dugdale-Barenblatt (D-B) model, sometimes also referred to as the “cohesive strip model”, has proved its usefulness in many applications. Initially developed to consider the mode-I plane-stress crack problem of ductile materials (Dugdale, 1960; Barenblatt, 1962), the D-B model has been extended to many other cases, for example, mixed mode cracks, fatigue, creep, damage and interface cracks (Janson, 1977; Yu and Fan, 1992; Mou and Han, 1994; Zhang and Gross, 1994; Becker and Gross, 1988).

Janson (1977) first introduced the concept of continuous damage into the D-B model and considered the damage in a narrow plastic zone ahead of a crack tip. Yu and Fan (1992) modified Janson's model by assuming that there is a narrow damage zone and a narrow plastic zone ahead of the crack tip. Adopting a damage model based on the hypothesis of incremental complementary energy equivalence, Mou and Han (1994) calculated the damage distribution near a crack tip. Zhang and Gross (1994) investigated a cohesive damage zone model of the D-B type for a mode-III crack in a power-law hardening material. Andersson (1977) presented a cohesive damage model consisting of a row of voids developed ahead of a

macrocrack tip to simulate the extension of the crack. For quasi-brittle materials, Feng and Yu (1995) investigated the effect of damage on fracture behaviour at a crack tip. It was pointed out that analogously to the plastic strip in a metal sheet (Dugdale, 1960); a fracture process zone is formed ahead of the crack tip in a solid.

As was mentioned above, coalescence of microcracks always occur in a quasi-brittle material before a fatal macroscopic crack forms. However, investigations on the coalescing process of microcracks are still very limited. In this chapter, the coalescence of interacting multiple collinear flaws in a rock is studied by using the analysis method of the Dugdale-Barenblatt model. As is usual for tensile failure, wing cracks at the end of the pre-existing flaw diminish their effects and become flatter in the case of randomly distributed flaws (Al-Ostaz and Jasiuk, 1997).

4.3 INITIAL FLAW FOR CRACK INITIATION AND BINOCULAR MICROSCOPE OBSERVATIONS

Micromechanical modelling of instability, mainly in underground mining, followed the development of analytical and computational fracture mechanics during the last four decades (Cherepanov, 1998), which allowed the understanding of the mechanisms and consequences of fracture initiation and growth. Observations of failure in physical experiments with cavities in brittle rocks (Santarelli and Brown, 1989; Ewy and Cook, 1990; Haimson and Song, 1993, 1998; Okland and Cook, 1998) suggest two main failure modes depending on the rock

microstructure: (a) microcrack accumulation; and (b) extensive fracture growth. A number of micro-mechanical models have been proposed with respect to these mechanisms. Shen et al. (1997) considered shear fracture development on the basis of the growth criterion that they had introduced prior to their work (Shen et al., 1993; Shen et al., 1994). Zheng et al. (1989) and Zheng (1998) considered borehole cross-section evolution based on a specially developed numerical scheme that mimics fracture of rock structural elements (spalls or chips).

Similarly, a number of works have considered buckling of layers (pre-existing or formed due to crack growth) as the main mechanism of borehole instability. These models were based on the micro-mechanical parameter of layer thickness, although the question of the layer appearance was usually left aside. This approach originated in composite mechanics for modelling delamination in compression (Kachanov, 1988) and is based on identifying the failure stress required for buckling of a thin surface layer of compressed material. In rock mechanics, this approach was adopted by Germanovich (1984, 1997) for modelling thermal spalling. Ortlepp and Stacey (1994), Bazant and Xiang (1997), van den Hoek et al. (1994) and Vardoulakis and Papamichos (1991) implemented the buckling approach for modelling rockbursts and breakouts. Although from different positions, Papamichos and Vardoulakis (1989) and Dyskin and Germanovich (1993) considered the coupling effect of surface instability and normal traction applied to the body surface and/or to the sides of the crack parallel to the surface. Bazant et al. (1993) proposed a model of borehole instability

based on simultaneous buckling of a package of layers of equal length. Bazant and Xiang (1997) subsequently used this approach to model shear bands consisting of slim columns (beams) between the locally growing cracks. Their approach seems to be adequate in the case of pre-existing layers with weak or no inter-layer cohesion.

Several authors have studied the influence of grain size on rock strength. Hugman and Friedman (1979) have shown that ultimate strength is inversely proportional to mean grain size in carbonate rocks such as limestones and dolomites. Olsson (1974) has also observed this trend in marble and has shown that the stress difference at failure is linearly proportional to the inverse square root of the mean grain size ($d^{-1/2}$). He suggested that the Petch theory (Petch, 1953) on the relation between yield stress and grain size in metals is also valid in polycrystalline aggregates, such as carbonate rocks. Fredrich et al., 1990, later confirmed a Petch relation in a variety of carbonate rocks of varying mean grain sizes.

It is commonly assumed that mean grain size in crystalline rocks (Fredrich at al., 1990; Wong et al., 1995) is a good measure of the initial Griffith flaw size in the material. With remote stress application, stress concentrations develop at the tips of the flaws, and maximum concentrations evolve at the crack tips, which are inclined at a critical angle with respect to the principal stress axes. Hatzor and Palchik (1997) have shown in heterogeneous dolomites that grain boundaries function as initial Griffith flaws

(Griffith, 1921; Bieniawski, 1967) in low-porosity rock (porosities ranging between 3-4%).

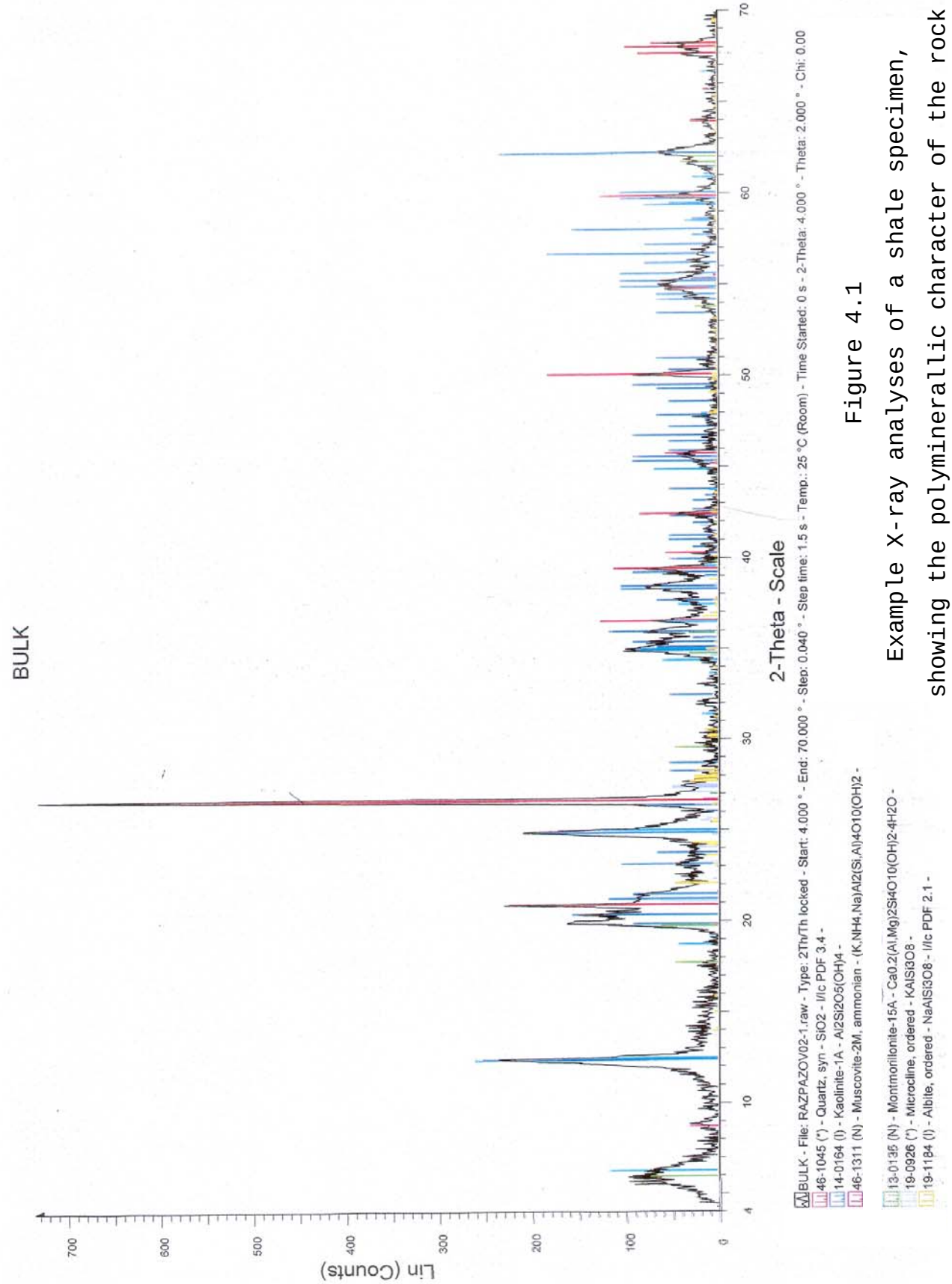

Figure 4.1 Example X-ray analyses of a shale specimen, showing the polymineralic character of the rock

X-ray analyses (Figure 4.1) of a shale specimen were conducted by the author to define minerals involved in the embedded shale layer. It was shown that the inclusion minerals, which form part of the investigated shale structure, are mainly quartz grains and carbon flakes, distributed in a mudstone matrix consisting of montmorillinite, kaolinite, muscovite, microcline and albite.

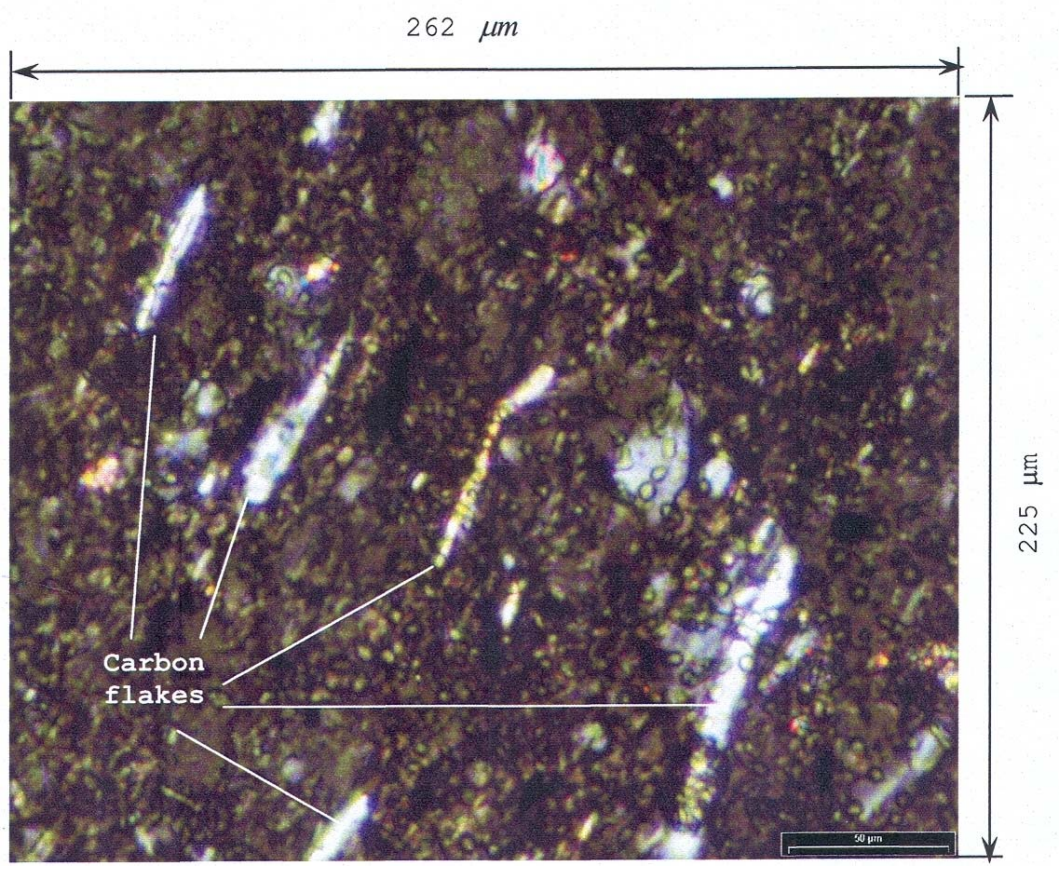

Picture 4.1
Symmetrically distributed carbon flakes in the shale specimen

For the detailed microscope measurements, thin sections of the shale layer were prepared. Of prime interest was the orientation of the carbon flakes in relation to the limb and highwall position. For these reasons an orientated diamond drill core of a shale layer situated

on the limb of an undulated strata formation was taken. The thin sections of shale specimens were cut parallel to the sedimentation and glued to the thin glass plates. After this, the glued shale material was polished to the thickness of about 30 μm and studied under a binocular microscope.

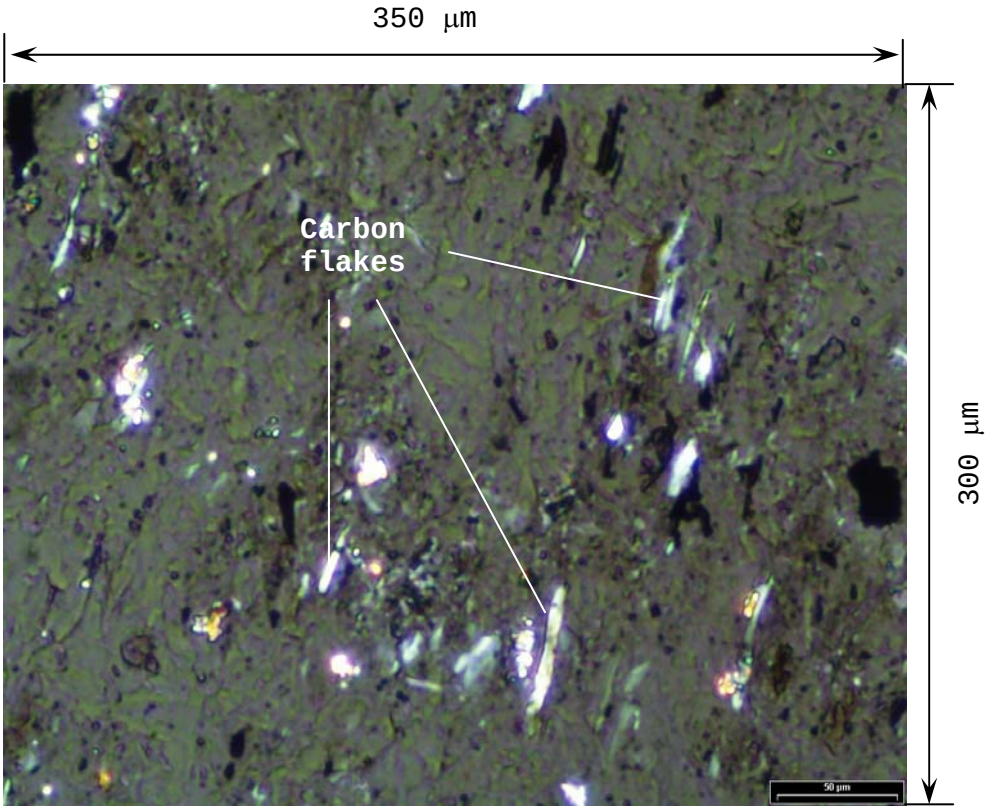

Picture 4.2

Carbon flakes with a length of between 8 μm and 21 μm

It was estimated that carbon flakes are parallel to sedimentation and symmetrically distributed in relation to each other (Picture 4.1) with an orientation almost normal to the highwall position and parallel to the limb inclination. As the flake lengths vary between 40 μm (Picture 4.2) and 110 μm (Picture 4.3), the average length was calculated to be 66 μm. The average thickness of the carbon flakes was measured at 5 μm.

The distance between the neighbouring flakes varies between 60 μm and 120 μm, with an average distance of 85 μm.

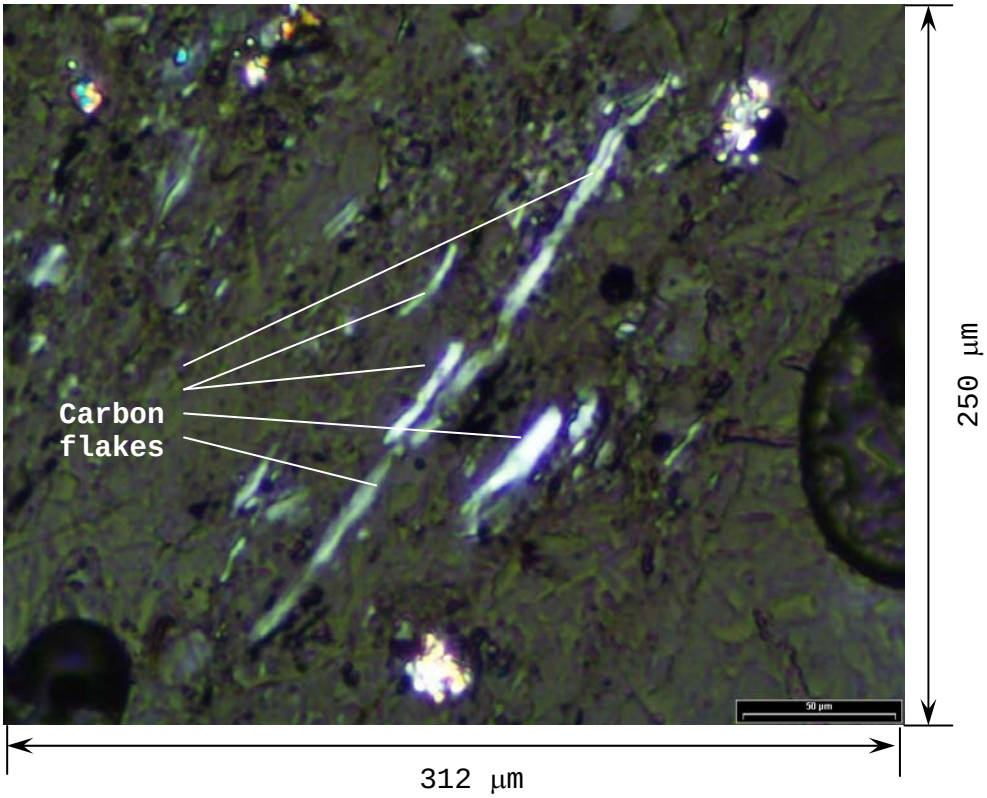

Picture 4.3

Carbon flakes with a length of between 30 μm and 190 μm

The second most common inclusion mineral in the shale is quartz, shown in Picture 4.4. It was estimated that average diameters of quartz grains are approximately 40 μm and that they are distributed randomly through the matrix at distances of between 110 μm and 230 μm apart. Hatzor and Palchik (1997) investigated the influence of grain size and porosity on crack-initiation stress and concluded that crack-initiation stress decreases from low porosity-high grain size to high porosity-high grain size. Their assumption of the

sliding crack mechanism in polycrystalline aggregates leads to the expectation that crack initiation and ultimate stress are linearly related to the inverse square root of the mean grain size, since existing grain boundaries are assumed to function as initial flaws, and therefore as stress concentrators (Petch, 1953). The longer the initial crack, the higher stress concentration and, therefore, the lower the remote stress level required for fracture initiation.

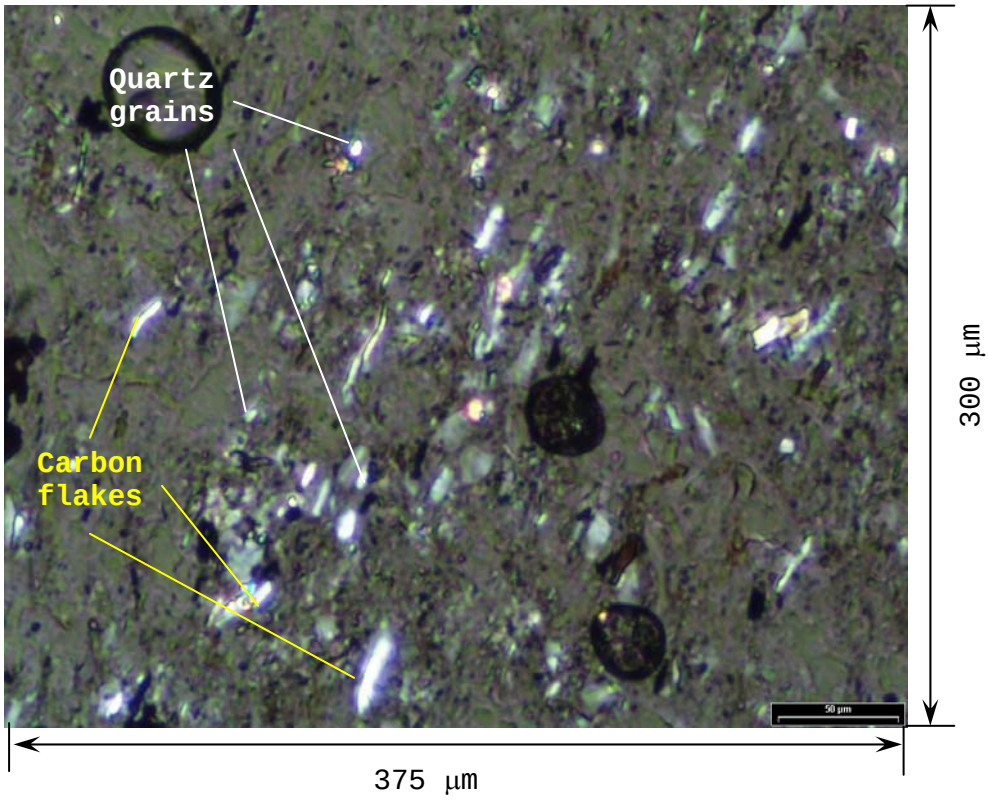

Picture 4.4

Carbon flakes and quartz grains in muddy matrix

4.4 MODE OF INTERACTION

As we observed, the carbon flakes and the quartz grains follow a certain loose order of distribution. As the most frequently seen inclusions in the shale thin sections, they definitely play an important role in the fracture-propagation process. It is assumed that the crack-inclusion separation and the size of the inclusion are small compared to the crack length, the outer end of which can be seen in every slope face. In the previous section we observed that the most common inclusions (carbon flakes and quartz grains) have different shapes, and will have different elastic moduli, to each other and the mud matrix. On the basis of smaller Poisson's ratio variations in rock and for model simplicity, it is assumed that the Poisson's ratios are the same and that the bonding between matrix and inclusions is perfect. Therefore, the crack is subjected to a remotely induced tensile stress field (see Chapter 3) specified by the applied stress-intensity factor, K_0. The near-tip field has the same classical form but its stress intensity factor, K_{tip}, is different, affected by nearby inclusions and the difference has the form of:

$$\Delta K_{tip} = K_{tip} - K_0. \qquad (4.1)$$

If we take into account the stress intensity factor for a single crack in a tensile stress field perpendicular to the crack line (Whittaker et al., 1992):

$$K = \sigma\sqrt{\pi c} \qquad (4.2)$$

where K is the stress intensity factor, σ is applied stress and c is the half of the crack length, then we can write Equation 4.1 as:

$$\left(\sigma_0 + \Delta\sigma_{tip}\right)\sqrt{\pi c} = \sigma_{tip}\sqrt{\pi c} \tag{4.3}$$

where the symbols σ_0, σ_{tip} and $\Delta\sigma_{tip}$ are the remote induced tensile stresses, the near-tip tensile stress, and the difference between them respectively. We can further simplify Equation 4.3 to:

$$\sigma_0 + \Delta\sigma_{tip} = \sigma_{tip} \tag{4.4}$$

where a negative value of $\Delta\sigma_{tip}$ predicts a toughening increment due to the shielding effect of the inclusions, and a positive $\Delta\sigma_{tip}$ means a weakening effect.

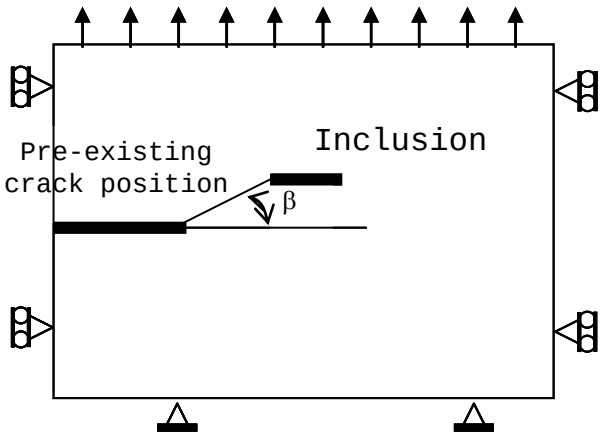

Figure 4.2
Applied boundary and stress conditions of the FLAC model for pre-existing crack and inclusion interactions (not to scale)

To investigate the interaction inclusions should have with an existing crack, the sizes of quartz grains and carbon flakes, discussed above, were taken into account. The microscope observations show that the angles between three carbon flakes and three quartz grains are not more than 12^0 and 15^0 respectively, shown by β in Figure 4.2.

FLAC was used for near-tip stress determination (model shown in Figure 4.2). Input values appear in Table 4.1, where the elastic moduli for the mudstone matrix and carbon flakes respectively come from van der Merwe (1998) and Markgraaff (1986). Both inclusion types were modelled at horizontal distances of 50, 100, 150, and 200 μm from the crack tip, while the angle β between the pre-existing crack plane and the inclusion centre-line, varies from 0.5^0 to 16^0.

Table 4.1 Input values for quartz grains and carbon flakes

	Mudstone matrix	Quartz grain	Carbon flake
Elastic modulus – E, GPa	7	70	4
Poisson's ratio - ν	0.25	0.25	0.25
Radius – R, μm	-	20	-
Length/width – l/W, μm	-	-	66/5
Distance from the cr. tip, μm	100, 150, 200 and 250		

In the models, the maximum zone length: width ratio of 10 was used to model the elongated shape of the cracks and carbon flakes. Taking this into account, the half crack was modelled by null zones. The pre-existing crack length was assumed to be 60 times the length of the carbon flake.

As the inclusion size is in the range of microns, the entire FLAC model was given dimensions of 1000 μm by 1000 μm (1 by 1 mm). The far-field stress was modelled with an applied pressure at the top boundary, normal to the X-axes and with a negative sign (to simulate tensile conditions). The inclusion position was modelled as defining certain zones into the model with the inclusion's properties, as shown in Table 4.1. The boundary conditions and the applied load are shown in Figure 4.2.

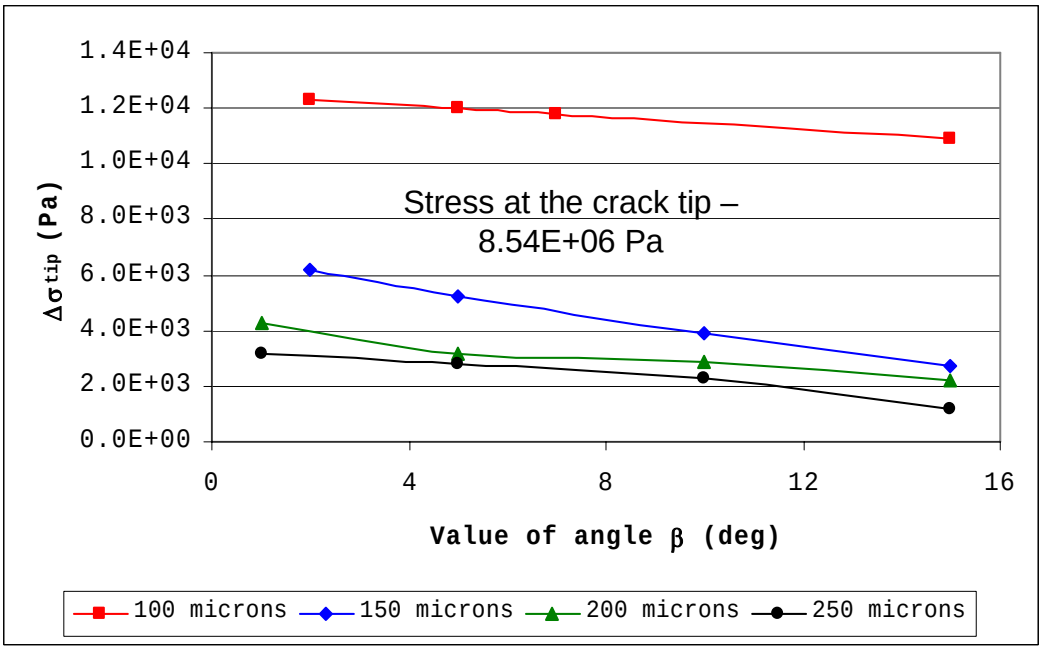

Figure 4.3

$\Delta\sigma_{tip}$ changes at the crack tip with carbon flake inclusions, according to the value of angle β and distance from pre-existing crack tip

Figures 4.3 and 4.4 present a plot of the FLAC model results for the $\Delta\sigma_{tip}$ interaction between the crack tip and carbon flakes and quartz grains respectively. These figures show only the results regarding the position of

the inclusions above the crack plane. If the inclusion is below the crack plane, the calculated stress difference is slightly lower compared to the inclusion's position above the plane. This difference can be explained by body forces in the material, but in both cases the stress difference ($\Delta\sigma_{tip}$) has the same sign.

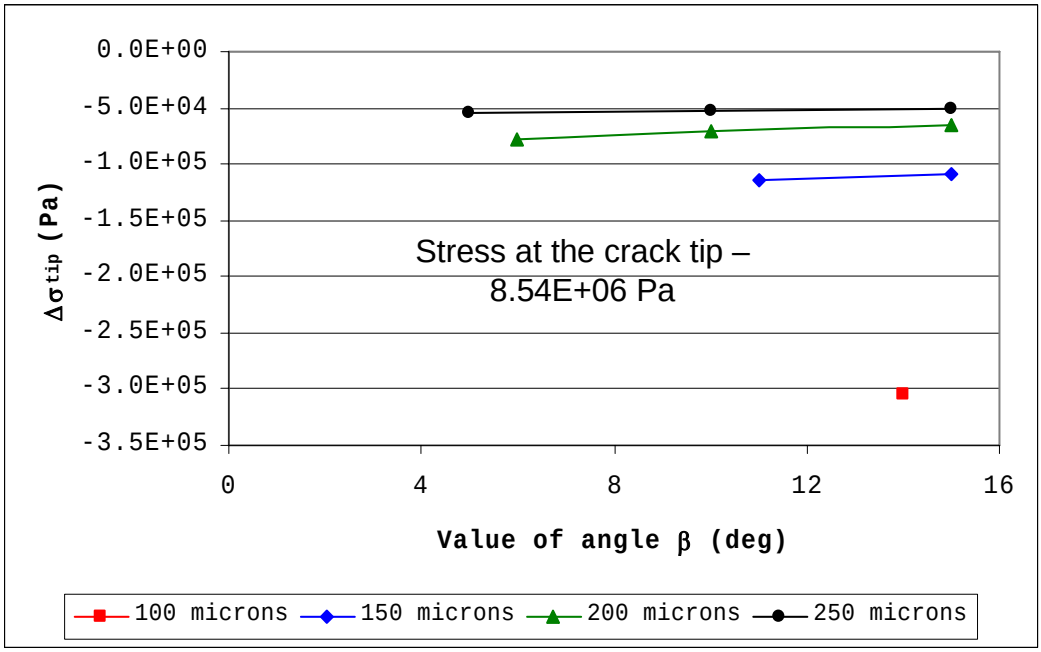

Figure 4.4

$\Delta\sigma_{tip}$ changes at the crack tip with quartz grain inclusion, according to the value of angle β

It can be seen (Figure 4.3) that all calculated results are positive and we can say that the carbon flakes weaken the mudstone matrix. In the figure, $\Delta\sigma_{tip}$ decreases with the increase in distance between the near flake end and the crack tip. From the all-modelled flake positions, $\Delta\sigma_{tip}$ has a maximum value at the lowest angle β in relation to the crack plane. These analyses are confirmed by the shale anisotropy, where

the elastic modulus normal to bedding is lower than the modulus parallel to bedding.

The quartz grains toughen the crack tip by inducing a negative value for $\Delta\sigma_{tip}$. Crack tip strengthening is much higher when the grain is closer to the crack tip (Figure 4.4) and this effect appears independent of the angle β between the grain and the fracture plane for the distances and angles investigated.

Figure 4.5 presents $\Delta\sigma_{tip}$ variations when the carbon flake (Figure 4.5a) and quartz grain (Figure 4.5b) are co-linear and at different distances from the pre-existing crack tip. There is general agreement between Figures 4.3 and 4.4 and Figures 4.5, and we can conclude that the presence of carbon flakes in the matrix will encourage fracture propagation, while the quartz grains will impede fracture propagation.

Therefore, any fracture propagation due to the remote induced tensile stress condition will involve more–or-less collinear carbon flakes, which behave as if they were cracks. If carbon flakes are distributed in the matrix in such a way that lines joining them are less than 12^0 inclined to the overall direction of the flakes, the interaction effects described above remain significant. This finding is valid only for the defined average flake size and average distance between flakes.

(a)

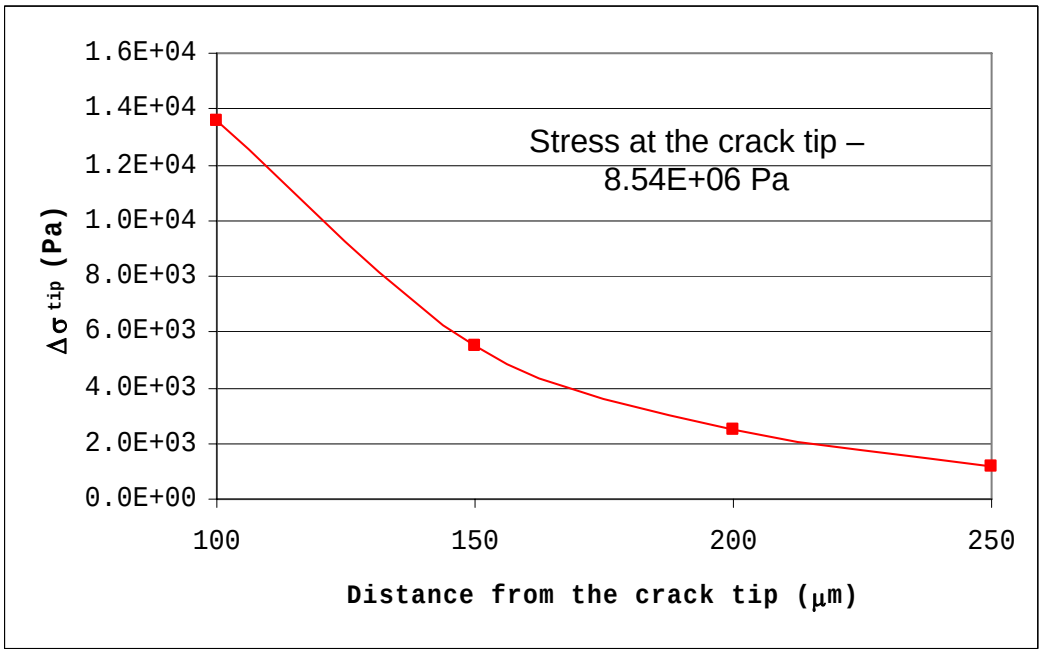

(b)

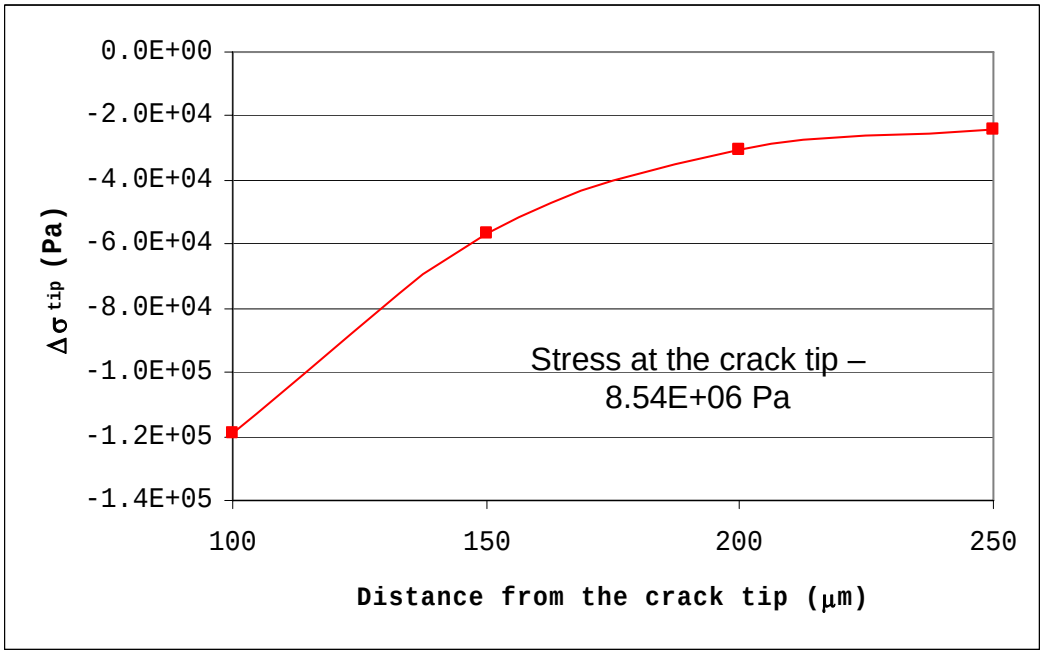

Figure 4.5

$\Delta\sigma_{tip}$ variation versus distance between the crack tip and a collinear carbon flake (a) and collinear quartz grain (b)

4.5 DEVELOPMENT OF SINGLE CARBON FLAKE-BASED CRACK MODEL FOR SHALE-COAL CONTACT

If the failure process is encouraged by the presence of carbon flakes in a mudstone matrix, then what remote stress condition has to be satisfied to induce the formation of a slip surface along the shale-coal contact? In this section, the general features and properties of cracks are gathered together into a simple crack model for the shale, and then this is extended to a row of collinear cracks in the next section.

Experimental observations suggest that one of the mechanisms of skin (strain) rockburst caused by tensile (splitting) fractures propagating, parallel to the major principal compressive stress direction (Fairhurst and Cook, 1966; Horii and Nemat-Nasser, 1985; Haimson and Herrick, 1986; Haimson and Song, 1993 and 1998; Van den Hoek et al, 1994 and Okland and Cook, 1998). These experiments refer to the splitting type of brittle fracture in compression, supporting a model in which a single crack extends, leading to failure. There are also observations which imply that there exist localized zones of multiple extensile cracks arising due to the interaction at the grain scale (Myer et al, 1992). These interactions result in an en echelon arrangement of growing cracks and might lead to structures characteristic for another common type of failure in compression, that is, oblique fracture (Germanovich et al, 1994). All these failures are more strain related and can not be explained with the stress-based criteria (e.g. Mohr-Coulomb, or Griffith). Stacey’s (1981) simple extension strain criterion for

fracture of brittle rock is empirical, as is the widely used criterion of Hoek and Brown (1980). Neither of these have any basis for general applications, unless there are observations and measurements to back an engineering judgement of failure. Failure criteria and their development lie beyond the scope of this thesis, and will not be considered any further. The author applies some fracture mechanics principles to achieve some practical results, in the hope of developing a plausible mechanism of fracture development along the shale – middle coal seam contact in the slope. This analysis begins first with a standard fracture mechanics approach, and then proposes a relaxation mechanism in a polyminerallic rock that could account for tensile failure even though the total stress state remains compressive.

In rocks, the crack-tip process zone is non-linear and is caused by the initiation and propagation of the microcracks in the immediate vicinity of the crack tip. Consequently, this zone is described as a microcracking zone, which appears and behaves in a similar way to the plastic zone in metals. It is actually a modification of Dugdale's (Dugdale, 1960) crack model originally developed for metals. Since there are no sound theoretical models available to fully describe the shape and size of the crack-tip fracture-process zone in rocks, the approximate models developed to describe the plastic zone in metals are often used.

Schmidt (1980) suggested a maximum normal stress criterion to describe the shape of the crack-tip fracture-process zone in rock. This criterion is based on the assumption that the formation of the fracture-

process zone takes place as a result of excessive tensile stress, i.e. when the local maximum principal stress in the vicinity of the crack tip reaches the ultimate uniaxial tensile strength of the rock. Thus

$$\sigma_1 = \sigma_t \tag{4.5}$$

where σ_t is the uniaxial tensile strength taken as positive to be consistent with the formulation of the crack-tip fracture-process zone.

It is known from the ISRM "Suggested methods for determining fracture toughness of rock" (Ouchterlony, 1988) that the testing results for fracture toughness generally should be corrected by a formula such as:

$$K_{IC} = \sqrt{\frac{1+p}{1-p}} K_q \tag{4.6}$$

in which K_q is the fracture toughness calculated using the linear elastic formula and p is a non-linear plasticity factor, which has been the subject of study of rock fracture toughness in recent years (Ouchterlony, 1988).

To calculate the plasticity factor, p, several unloading-reloading cycles must be conducted in the fracture-toughness testing process of rock according to the ISRM methods (Ouchterlony, 1988). The p factor represents the ratio of irreversible deformation and is calculated as shown in Figure 4.6:

$$p = \frac{\Delta\delta_i}{\Delta\delta_p} \tag{4.7}$$

It was found by experiment that the p factors for metal specimens were close to zero when their diameters were small (Barker, 1979). The p factors of rock specimens are typically larger than 0.10 (for coal – 0.32; sandstone – 0.28; quartz – 0.16; norite – 0.18, after Karparov, 1998). Because of the friability of the shale layer above the coal, it was not possible to obtain a reliable p factor in the laboratory. The p factor was found to be a constant for rock specimens with diameters over 30mm (Whittaker et al., 1992).

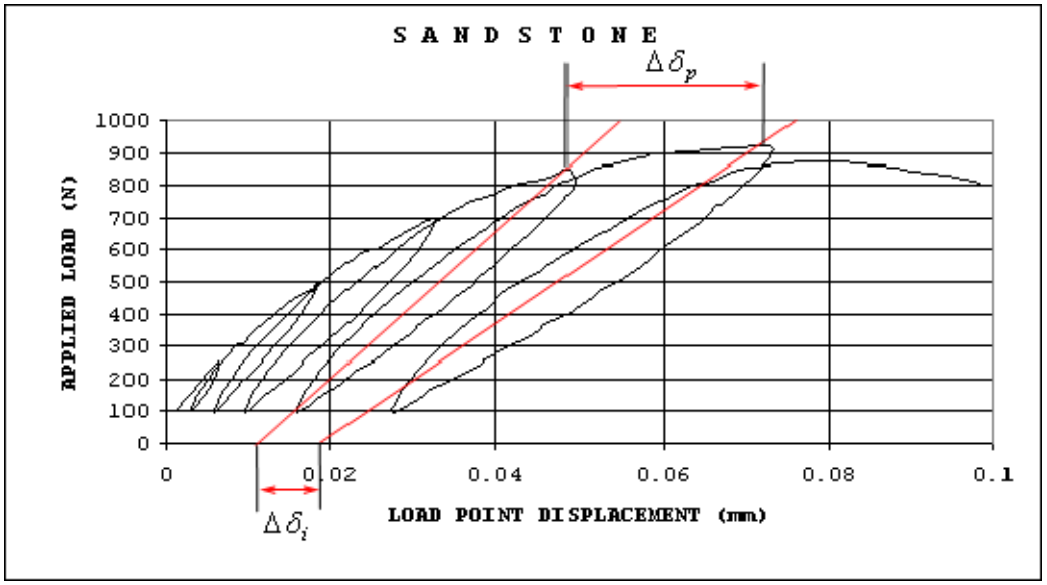

Figure 4.6
Calculation on plasticity factor "p" for sandstone specimen (after Karparov, 1998)

According to the micromechanical damage theories for brittle and semi-brittle materials (Krajcinovic, 1997; Nemat-Nasser and Horii, 1993; Dugdale, 1960; Barenblatt, 1962; Janson, 1977; Yu and Fan, 1992; Mou and Han, 1994; Zhang and Gross, 1994; Becker and Gross, 1988; Andersson, 1977; Xia et al, 1995; Feng and Yu, 1995), there exists a distributed damage zone around a

crack tip, where some microcracks that satisfy a specific growth criterion propagate in a stable manner.

The cohesive crack model is based on the assumptions made by Labuz et al. (1987), Ingraffea and Gerstle (1984), and Carpinteri et al. (1986). In general, the stress-strain relation of such a material can be divided into three stages: linear elasticity, plastic behaviour, and strain softening. In some papers (Bui and Ehrlacher, 1981; Bui et al., 1984; Hao et al., 1991), a completely damaged fracture process zone with a specific shape, and which cannot sustain any small stress, was assumed.

When the applied load reaches a limit value, damage will be localised in the direction perpendicular to the maximum principal stress. Once the damage localisation occurs, the stresses near the crack tip will be partly released. Instead of the completely damaged zone with finite sizes, therefore, the fracture process zone reflects some more realistic features of damage at the crack tip in rock. Moreover, less energy will be dissipated during the crack propagation with a fracture-process zone than with a completely damaged zone of a specific finite width (Feng and Yu, 1995).

The crack damage stress is generally referred to as the stress at onset of dilation. Until this stress level is reached, the rock volume decreases. When the crack damage stress has developed, the material volume begins to increase (Bieniawski, 1967; Schock et al., 1973; Brace, 1978; Paterson, 1978; Brady and Brown, 1993). Martin and Chandler (1994) and Eberhardt et al. (1999)

have used the term "crack damage stress σ_{CD}" and have shown that rocks become critically damaged at σ_{CD}, which is significantly lower than the failure stress.

Using an elastic-rapid damage model, for example, Bui and Ehrlacher (1981) obtained the solution of damage for a steady-state propagating crack shown in Figure 4.7b. Their solution is equivalent to the configuration of a steadily extending notch in an infinite sheet. Generally, the shape of the carbon flakes is not the same (see Figure 4.7a). Even if carbon flakes have a similar shape in their original state, they will not keep this shape during fracture initiation and propagation due to the chaotic microstructural disorder of grains in the rock matrix.

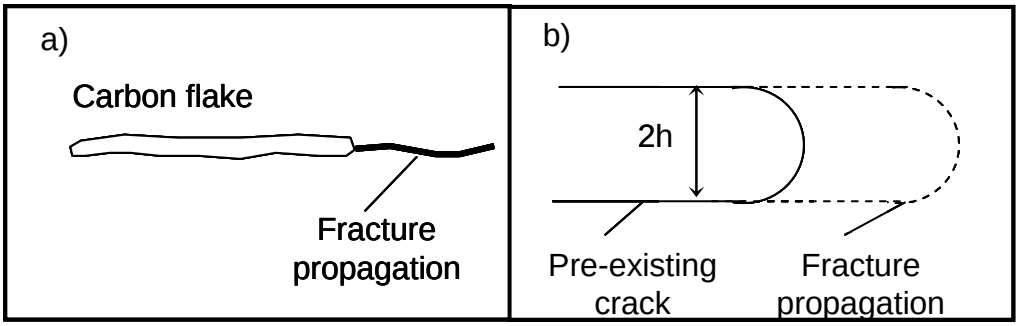

Figure 4.7
(a) Fracture propagation in the rock specimen from carbon flake, which behaves like a pre-existing crack; (b) Model of steady state fracture propagation after Bui and Ehrlacher (1981)

For the shale, a notional crack with an effective crack length is assumed equal to the average carbon flake length of 66μm. This effective crack length consists of a tensile free point (true crack length) and a length

of fracture-process zone over which a cohesive stress, tending to close the crack, is distributed. Such a hypothesis is often referred to as a "fictitious crack".

This study uses additional assumptions regarding the remote stress distribution over the grain boundaries and grain orientation, due to the bedding inclination on the undulated strata formation limb:

1. The carbon flake orientation is parallel to the bedding.
2. Taking into account flake size and stress changes in a slope profile, it is assumed that a remote tensile stress difference ($\Delta\sigma_N$) is a constant and is uniformly distributed over a large number of grains.
3. The material in the fracture-process zone is partially damaged but still able to carry stress $\sigma(x)$, which is transferred from one surface to the other of the rock, while the material outside the fracture process zone is assumed linearly elastic.
4. The fracture process zone starts to develop when the stress difference $\Delta\sigma_N$ normal to bedding reaches the tensile strength σ_t and the corresponding true crack-tip opening displacement δ_t is zero. With increasing δ_t, the stress is decreased until zero and the corresponding δ_t reaches a critical value δ_c. Such a phenomenon of decreasing stress with increasing deformation is known as strain-softening behaviour (Hilleborg, 1985) or tension-softening behaviour (Horii et al., 1987; Leung and Li, 1987).

5. The closing cohesive stress is a function of true crack-tip opening displacement δ_t, i.e. $\sigma(x)$, which is the Dugdale crack model where the closing cohesive stress $\sigma(x)$ is assumed to be a constant, having the value of the yielding strength.
6. The overall stress intensity factor at the notional crack tip no longer exists, i.e. the stress singularity at the notional crack tip disappears.

To determine conditions favourable for crack propagation, it is essential to choose an appropriate fracture parameter and thereby to establish an applicable fracture criterion (see Figure 4.8). Before loading, the crack length is $2a$. From the above discussion, it can be seen that damage localisation occurs ahead of the two tips of the crack in tension.

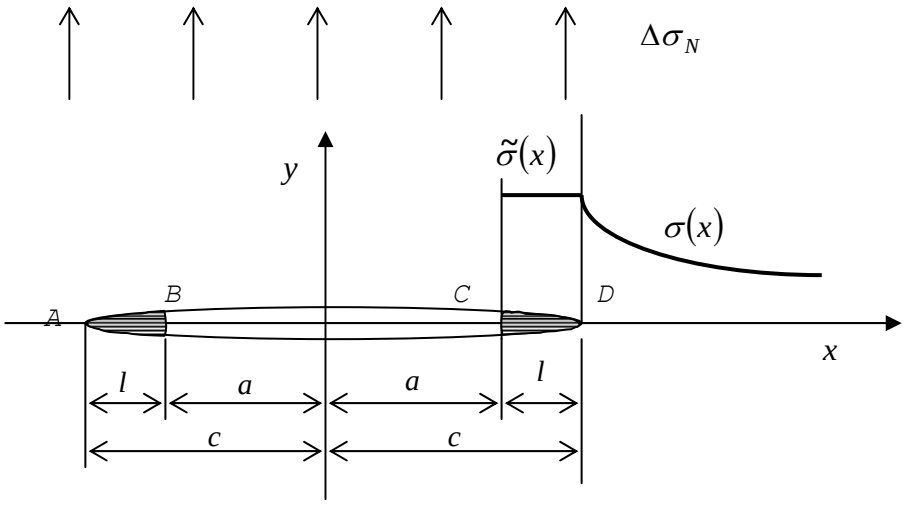

Figure 4.8
Fracture-process zone localisation of a flaw under tension

The material in the fracture-process zone experiences a stress drop and strain softening but still has a

certain amount of residual strength to maintain the stresses. Thus, the equivalent crack length is $2c = 2(a+l)$ with l denoting the length of the fracture-process zone. The normal stress in the ***y*** - direction along the ***x*** - axis is expressed as:

$$\sigma_{yy} = \begin{cases} \tilde{\sigma}(x) & (a \le x \le c) \\ \sigma(x) & (x > c) \end{cases} \qquad (4.8)$$

The compatibility condition of deformation requires at x=c that $\tilde{\sigma}(c) = \sigma(c)$, that is, the stress $\Delta\sigma_N$ is continuous. In D-B models, the material-specific decreasing tensile stress versus the increasing displacement difference between the zone faces usually characterises the cohesive damage zone. According to Schmidt (1980 – given in Equation 4.5), it will be assumed that the tensile stress remains constant at the value σ_{tt}, equal to the strength σ_t within the cohesive zone, that is,

$$\tilde{\sigma}(x) = \sigma_t \qquad (a \le x \le c) \qquad (4.9)$$

Under the external tensile stress $\Delta\sigma_N$ (discussed in Chapter 3), the stress intensity factor of the equivalent crack with length $2c$, Equation 4.2 can be written by analogy as:

$$K_I^N = \Delta\sigma_N \sqrt{\pi c} \qquad (4.10)$$

By requiring that the stress intensity factor at the fictitious crack tips ($x = \pm c$) disappears, that is,

$$K_I^N + K_I^D = 0 \tag{4.11}$$

In the linear elastic fracture mechanics, the stress intensity factor is often adopted as the control parameter for determining the crack propagation. Then, the fracture criterion for a mode-I crack is

$$K_I^N = K_{IC} \tag{4.12}$$

with K_{IC} being the matrix fracture toughness. For a crack of length $2a$ in an infinite plate under an external tensile stress (Figure 4.8), the critical stress corresponding to the crack propagation is obtained as

$$\sigma_N^c = \frac{K_{IC}}{\sqrt{\pi a}} \tag{4.13}$$

The fracture criterion given by Equation 4.12 has been extensively used (Broek, 1996; Kanninen and Popelar, 1985). The corresponding fracture criterion takes the form

$$l = l_c. \tag{4.14}$$

4.6 PERIODIC COLLINEAR CRACK MODEL FOR SHALE-COAL CONTACT

The following problem to be considered is that of a periodic row of co-linear carbon of equal length $2a$ (the length of the average flake) in an infinite space subjected to a remote induced tension, $\Delta\sigma_N$ (discussed in Section 3.8), and shown in Figure 4.9.

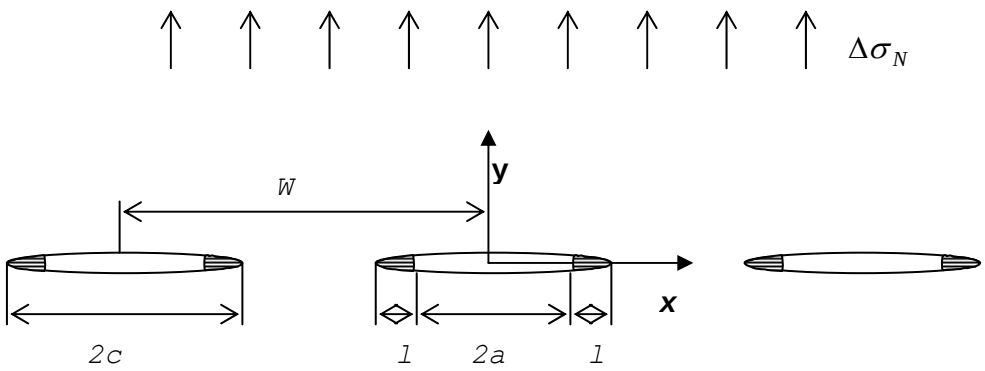

Figure 4.9
Simplified model of a periodic row of collinear carbon flakes in shale

The stress intensity factor at each flake tip caused by the remote induced tension is (Tada et aI., 1985).

$$K_I^N = \Delta\sigma_N \sqrt{W \tan\frac{\pi c}{W}} \qquad (4.15)$$

where $c = a + l$ denotes the half-length of the equivalent flakes, and l the length of the fracture process zone. When each flake is subjected to two pairs of symmetrical concentrated forces, $-\sigma_t d\xi$, normal to the crack surfaces and acting at $x = \pm\xi$, the stress intensity factor at each crack tip is (Tada et al., 1985)

$$dK_I^D = -2\sigma_t\, d\xi \cos\frac{\pi\xi}{W}\sqrt{\frac{1}{W}\tan\frac{\pi c}{W}}\left[\left(\sin\frac{\pi c}{W}\right)^2 - \left(\sin\frac{\pi\xi}{W}\right)^2\right]^{-\frac{1}{2}} \qquad (4.16)$$

By integration (see Appendix 1 – A1.3.1), the stress intensity factor induced by the stress σ_t in all the fracture-process zones is:

$$K_I^D = -2\sigma_t \sqrt{\frac{1}{W}\tan\frac{\pi c}{W}} \int_a^c \cos\frac{\pi\xi}{W}\left[\left(\sin\frac{\pi c}{W}\right)^2 - \left(\sin\frac{\pi\xi}{W}\right)^2\right]^{-\frac{1}{2}} d\xi$$
$$= -\sigma_t \sqrt{W\tan\frac{\pi c}{W}}\left[1 - \frac{2}{\pi}\arcsin\frac{\sin(\pi a/W)}{\sin(\pi c/W)}\right]. \qquad (4.17)$$

Substituting Equation 4.15 and 4.17 into the finiteness condition of Dugdale:

$$K_I^N + K_I^D = 0, \qquad (4.18)$$

the length of the fracture-process zone is obtained as (see Appendix 1 – A1.3.2)

$$l = \frac{W}{\pi}\arcsin\frac{\sin(\pi a/W)}{\cos(0.5\pi\,\Delta\sigma_N/\sigma_t)} - a. \qquad (4.19)$$

With an increase in $\Delta\sigma_N$, the length of the fracture process zone increases. We can use again Equation 4.13 to calculate the critical fracture process zone length in the case of a periodic row of flakes. Then Equation 4.19 will have the form of

$$l_c = \frac{W}{\pi}\arcsin\frac{\sin(\pi a/W)}{\cos\left(\frac{K_{IC}}{2\sigma_t}\sqrt{\frac{\pi}{a}}\right)} - a \qquad (4.20)$$

From Equation 4.20 and the fracture criterion – Equation 4.14 - the critical stress of $\Delta\sigma_N$ corresponding to the crack propagation is arrived at (see Appendix 1 – A1.3.3):

$$\sigma_N^p = \frac{2\sigma_t}{\pi} \arccos \frac{\sin(\pi a / W)}{\sin[\pi(a + l_c)/W]}. \qquad (4.21)$$

Once $\Delta\sigma_N$ reaches σ_N^c, the collinear flaws propagate and begin to coalesce as a result.

It is also seen that when the length of the collinear flaws is bigger than the characteristic value

$$a_c = \frac{1}{2}W - l_c \qquad (4.22)$$

the collinear flaws may also coalesce due to the linking of two fracture-process zones, even though $\Delta\sigma_N < \sigma_N^L$. Therefore, another condition for flaw coalescence is:

$$2c = 2a + 2l = W \qquad (4.23)$$

Substituting Equation 4.19 for Equation 4.23 leads to the critical tensile stress of the fracture-process zone linking as follows (see Appendix 1 – A1.3.4):

$$\sigma_N^L = \sigma_t \frac{(W - 2a)}{W}. \qquad (4.24)$$

For a periodic array of collinear flaws of equal length in an infinite sheet, thus, the stress of flaw coalescence is:

$$\sigma_N^p = \begin{cases} \dfrac{2\sigma_t}{\pi} \arccos \dfrac{\sin(\pi a / W)}{\sin[\pi(a + l_c)/W]} & \text{for } a < a_c \\ \sigma_t \dfrac{(W - 2a)}{W} & \text{for } a > a_c \end{cases} \qquad (4.25)$$

Up to now, we have worked in the field of elasticity. The calculated critical tensile stress has to be corrected with a plasticity indicator (Equation 4.6) to be applicable to the ductile properties of most sedimentary rocks. Hence, from Equation 4.13 we can write:

$$K_{IC} = \Delta\sigma_N^P \sqrt{\pi a} \tag{4.26}$$

Combining Equations 4.26 and 4.6 we have:

$$K_q \sqrt{\frac{1+p}{1-p}} = \Delta\sigma_N^P \sqrt{\pi a} \tag{4.27}$$

and consequently

$$K_q = \frac{\Delta\sigma_N^P}{\sqrt{\frac{1+p}{1-p}}} \sqrt{\pi a} \tag{4.28}$$

Then Equation 4.25 can be rewritten in the same form by analogy as dividing the tensile strength (σ_t) by the coefficient $\sqrt{\frac{1+p}{1-p}}$. Hence, Equation 4.25 will have the form of:

$$\sigma_N^p = \begin{cases} \dfrac{2\sigma_t}{\pi\sqrt{\frac{1+p}{1-p}}} \arccos \dfrac{\sin(\pi a / W)}{\sin[\pi(a + l_c)/W]} & \text{for } a < a_c \\ \dfrac{\sigma_t}{\sqrt{\frac{1+p}{1-p}}} \dfrac{(W - 2a)}{W} & \text{for } a > a_c \end{cases} \tag{4.29}$$

These equations are applied to the carbon flakes in the mudstone matrix in the following Section.

4.7 DETERMINATION OF THE CRITICAL TENSILE ZONE LENGTH ALONG THE UPPER AND BOTTOM SHALE CONTACT SURFACES

In Chapter 3 (Figure 3.9) we calculated the normal stress difference ($\Delta\sigma_N$) along the failure surface. In this chapter (Section 4.3) we estimated the average length of carbon flakes ($66\,\mu m$) and the average distance between them ($85\,\mu m$). Hence, we are in a position to calculate the magnitude of the critical tensile stress for fracture propagation in terms of $\Delta\sigma_N$ along the potential failure plane. Because of the flaky quality of the shale under study, it was impossible to drill an intact core for the Mode-I stress intensity factor (K_{IC}) estimation. For this reason in the following calculations, the author accepts experimental results by Schmidt (1977), Bhagat (1985), and Atkinson (1987) for the shale stress-intensity factor, K_{IC}=$0.94\,MPa-m^{-1/2}$ and plasticity indicator, p = 0.33. Then, the critical fracture-process zone for the periodic crack row has the length $l_C = 4.91\mu m$ (Equation 4.20).

If we compare the critical half carbon-flake length ($70.1\,\mu m$ - Equation 4.22) with the average measured flake half length ($33\,\mu m$) then tensile fracture propagation is the result of the remote applied tensile stress. After Equation 4.29, we calculate the critical tensile stress $\Delta\sigma_N^P = 0.210MPa$ for the periodic row of flakes for the shale. Figures 4.10 and 4.11 present the plot of the stress normal to bedding and the

critical (σ_N^P) tensile stresses of the embedded shale layer in the upper and the bottom contact surfaces. The stress state shown in Figure 4.11 is the same as in Figure 3.21.

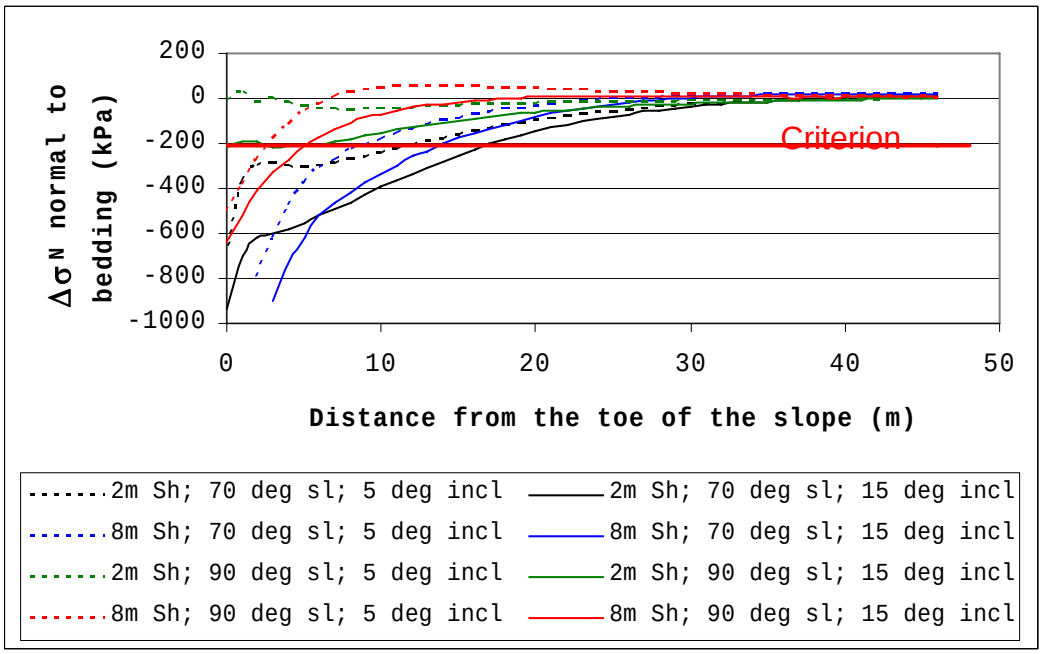

Figure 4.10

Critical tensile stress value - σ_N^P (bold red line), with the stress differences normal to bedding at the upper shale contact

Figure 4.10 shows for the upper shale contact that only the vertical slope with 2m-thick embedded layer dipping at 5^0 does not have the conditions for tensile fracture propagation due to the $\Delta\sigma_N$ value. The bottom contact is affected by $\Delta\sigma_N$ in slope profiles with a 15^0 inclination. This encourages the growth of a tensile crack along the coal-shale contact. The modelled tensile fracture lengths appear in Table 4.2.

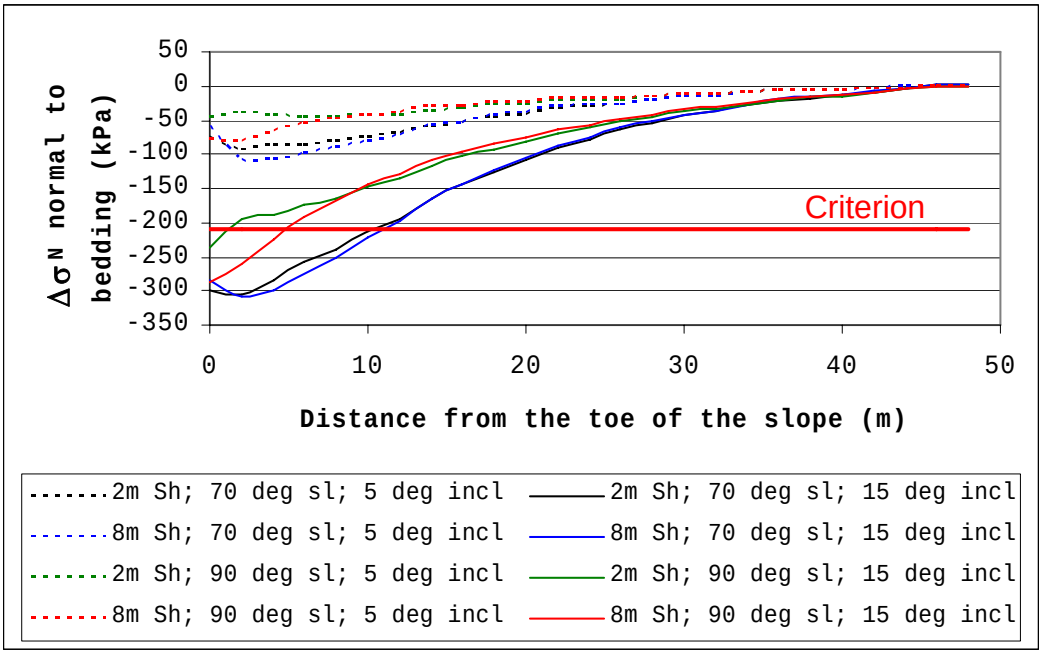

Figure 4.11

Critical tensile stress value - σ_N^P (bold red line) with the stress differences normal to bedding at the shale-middle coal seam contact

Table 4.2 Potential Lengths of the tensile fractures along the contact surfaces between the embedded shale layer with the overburden and the bedrock

	Slope angle (^{0})	5^0-limb inclination		15^0-limb inclination	
		2m thick	8m thick	2m thick	8m thick
Top contact	70	12m	8m	16m	14m
	90	0m	4m	6m	6m
Bottom contact	70	0m	0m	12m	12m
	90	0m	0m	2m	6m

The tensile fracture zone along the top contact surface is longer than that along the bottom contact surface. This is the result of the higher relaxation at the upper shale contact compared to the lower shale contact. For better visualisation, the lengths of the tensile fracture zones along the top and bottom contact surfaces can be seen in Table 4.2, which show that the slope profile with flatter slope angle creates longer tensile zones compared to the profile with steeper slope angle. This may explain why the major failure in Colliery – A1 took place after the minor failure, which had resulted in a reduction of the slope angle (see Chapter 1).

4.8 DISCUSSION AND CONCLUSIONS

The following conclusions can be drawn from the attempt to explain the genesis of the failure surface along the shale – middle coal seam contact that has been observed in all three major slope failures at the coal mine. Firstly, failure processes in solids are not well understood, and although the fracture mechanics approach has produced some excellent results, it is still unable to completely explain failure in rock. This study has approached the problem of determining if there is a possibility of generating a tensile failure surface close to, or on the bottom shale contact with the coal, in a stress regime in which the stress normal to the surface remains compressive, after there is a net relaxation as the slope is cut.

There are two points of interest concerning the development of the failure surface:

- Excavations in deep level mines become unstable once the surrounding stress has been relaxed for whatever reason (this is called unravelling), but the failure surfaces had already formed prior to the relaxation, and not during the relaxation;
- The shale thin sections were taken from the body of the shale, and not on the shale-middle coal seam contact itself, where in all likelihood, carbon flake density and alignment are likely to be increased and more consistent respectively, thereby reducing the critical tensile stress required to produce tensile failure, according to the above analysis.

The failure could conceivably start at the slope toe where stress relaxation is total, and then progress into the slope interior along the bottom contact in a mixed-mode fashion. This is perhaps more likely because the strata inclination is important: significant collapses have only taken place on limb inclinations of approximately 15°. Post-collapse observations have not been able to determine whether the failure surface formed in tensile, shear, or mixed-mode fashion, because shear displacement took place along it in all cases during the slope collapse.

Some of the outcomes in this chapter provide valuable insights, and are listed below:

- Carbon flakes weaken the mudstone matrix, and because of their weaker properties compared with the other minerals, must be involved in the genesis of the failure surface.

- As a result, we can define two regions on the failure surface: the first, where failure by whatever mechanism has developed (probably from the toe into the slope), and which is defined as the frictional region; the second, which lies beyond the first, where the normal stress relaxation is too small to permit further fracture growth, and this is called the cohesive region.
- The frictional zone length has an inverse relationship with the slope angle, i.e. it extends further into the slope interior for flatter slope angles than for steeper slope angles.
- The frictional zone length will be related to the limb inclinations, the limb lengths, and pore water pressure.
- A stress-based failure criterion has been used, but this fails because the net vertical stress remains compressive. A strain-based criterion would perhaps be more successfully applied in this case, and research to determine a suitable criterion should be initiated.

Even though this study has not been able to determine the failure mode absolutely, a fracture mechanics approach shows that even partially aligned carbon flakes will weaken the shale at the shale-middle coal seam contact, encouraging the formation of a failure surface along this contact, whose stability will ultimately depend purely on friction. No attempt was made in the analyses to predict how quickly such a failure surface will form after the mining slope has been cut. Although there are no records at the mine detailing time-spans between slope creation and slope

failure, best estimates based on experience range between two to four months (Mattushek, 2005).

The mode of fracture formation is also not detectable from the exposed failure surfaces, because subsequent slip of the overlying strata had taken place along them after the slopes had reached an unstable condition. The detailed nature of the fracture formation mechanism is not of critical importance to the outcome of the work, because we know from observation that the failure surface must form by whatever mechanism, either in part or all of the intervening period between slope formation and ultimate failure, or in the few instants before slope collapse. The actual mode and mechanism of failure surface formation continues to remain unknown, and fracture mechanics demonstrates that a stress-based approach is inappropriate.

The initial objective of this work was to explain why the accepted slope stability analysis methods were unable to predict the failures, and to produce a more reliable method of slope stability analysis in the conditions seen at the mine. In the following chapter, we accept that a failure surface grows in time along the shale-middle coal seam contact because the fracture analyses do not prohibit the formation of a fracture along the shale-middle coal seam contact, and DIGS modelling favours the formation of a fracture near the contact. Because of either progressive or sudden weakening of the contact, a sufficiently large frictional region must form to allow eventual slope collapse.